

Contents

1	Introduction	3
2	Numerical PDE Solution to HIV Trapping in Cervico-Vaginal Mucus	3
2.1	Background	3
2.2	Model	4
2.2.1	Numerical Approximation to Solution	6
2.3	Transport Scaling Analysis	8
2.4	Virion Infectivity	9
3	Multi-Scale Model of Axonal Transport	14
3.1	Background	14
3.2	Model	14
3.2.1	QSS Reduction of the CK Equation	16
3.2.2	Analytic and Numerical Solutions	17
3.3	Kinetic Properties of System on Overall Transport	18
3.4	Maximization of Effective Transport	20
4	Conclusion	21
5	Acknowledgements	22

1 Introduction

A variety of biological systems utilize so-called crosslinking proteins. The two relevant examples discussed in this work are antibodies (Ab) and molecular motor proteins. Both are similar in overall structure; they are generally small and "Y" shaped with the same binding region in each of the forks, and a different region at the base. However, their functions are markedly different. Ab are immune proteins that live outside cells and perform a large number of protective tasks, whereas molecular motors are transport proteins that reside in the majority of cells and are used primarily for transport.

Recent studies in various biological processes have shown that fast, short-lived interactions between crosslinking proteins and their ligands improve outcomes when cooperation among crosslinkers is involved [5, 9]. This is directly against the long-standing thought that creating a long-lasting bond would improve outcomes by increasing the amount of time that the crosslinker interacted with their ligand.

To aid in the experimental understanding of the short-lived crosslinking phenomenon, computational models on a variety of scales, from population-scale PDEs to single-molecule stochastic models of chemo-mechanical cycles, have been created to simulate the systems [8, 9, 11]. Here, we discuss primarily a differential equation model describing reaction, advection, and diffusion of molecules through their systems, with some focus on underlying stochastic processes. This work is broken up into two sections for each biological setting examined. Section 2 focuses on the antibody model and Section 3 focuses on the molecular motor model. We discuss the unique biological situations of antibodies and molecular motor proteins, define the relevant equations describing the motion and interaction of the specific particles, and define parameters that determine the "effectiveness" of the biological system. We then discuss the numerical approximations to the solution of the PDEs and their computation. Binding characteristics are then adjusted to determine the characteristics of the most effective systems.

2 Numerical PDE Solution to HIV Trapping in Cervico-Vaginal Mucus

2.1 Background

Antibodies (Ab) are vital components to the body's immune response. They are manufactured by B cells such that the fork region of the Y (the Fab region) binds with high specificity to a particular epitope found on the infective particle (i.e. a bacteria or virion), while the base (the Fc region) binds to other proteins and cell receptors in the body. The immune system utilizes antibodies for a number of processes that search for and destroy foreign objects. These range from flagging phagocytes, to initiating processes used to puncture membranes, to starting immune responses when reinfections occur [4].

Antibodies also have protective functions outside the body's tissues. It is common for certain forms of antibody to exist in large quantities in mucus layers beyond the body (i.e. the respiratory tract and cervico-vaginal mucus layer (CVM)) [4]. The prevailing theory has been that antibodies have time to accumulate on foreign particles before they enter the body

to minimize their potential for damage [2]. However, it has been recently shown in the Lai research group that the Fc region possesses a weak affinity to mucin polymers; this affinity allows trapping of infective particles, namely HIV virions, beyond the body [10]. They show that a weak affinity is necessary to maximize trapping, as opposed to a strong affinity that would keep HIV from moving any farther once trapped the first time. The basis for this theory lies in the fact that more free antibodies are better able to bind to virions, which has a two-fold effect. First, a multi-Ab virion complex is better able to keep a virion bound to mucin than a single Ab. Second, more Ab on a virion that does enter the body has less epitopes with which to mount an infection, thus minimizing the overall potential for harm.

In the group’s previous model for HIV virion and antibody movement in a one dimensional view of the cervical/vaginal mucus (CVM) and seminal layer have given a good understanding of penetration into the body [11]. In this model, virions and antibodies move under the influence of diffusion. Antibodies that diffuse into the seminal layer are able to bind and unbind to HIV at given rates. This does not change a virion’s diffusive properties in the semen because the size of antibodies is far smaller than that of a virion. However, the number of antibodies on virions affects a virion’s ability to diffuse through the mucin layer, as interactions between antibodies and mucin cause the virion to become stationary until all Ab detach.

In this work, movement of antibodies and virions towards the cell wall was added. A difference in osmolarity between mucin and semen creates a pressure difference that causes water to flow towards the cell layer and out of the semen. Therefore, all antibodies and virions within this fluid will want to move towards the cell wall. We also added the ability for semen to drain out of the system due to liquifaction of the fluid. This project was conducted over four years under the direction of Dr. Timothy Wessler (University of Michigan). The information presented here is my contribution to the project and work under preparation for submission.

2.2 Model

We model the vagina as a hollow cylinder with a height of 62500 μm . The cervix is defined to be the top of the cylinder, $z = 0$, and the introitus at the bottom, $z = 62500$. We treat the cell layer as our outermost radial boundary condition and model a two-layer system as follows. Antibodies begin in the CVM, which is on average a 50 μm layer coating the vaginal cell layer. We assume that semen is deposited uniformly throughout the entire geometry, resulting in a 200 μm layer directly over the CVM. The semen interfaces directly with air in the innermost radial boundary.

Ab and HIV virions are assumed to be initially uniformly distributed in the CVM and semen respectively. Because of differences in concentrations, antibodies and virions will tend to diffuse into the other layer with free diffusivities $D_{\text{Ab}} = 40 \mu\text{m}^2 \text{s}^{-1}$ and $D_{\text{vir}} = 1.27 \mu\text{m}^2 \text{s}^{-1}$ respectively. Antibodies and virions freely bind and unbind to each other at rates k_{on} and k_{off} respectively. Antibodies bind to epitopes arranged as trimers on the surface of the virions, so a virion with N^* trimers has $3N^*$ Ab binding sites. Experimental evidence has shown that the number of trimers on virions falls between 4 and 35 and is distributed in a Negative Binomial fashion with parameters $r = 28/5$ and $p = 5/7$ [12]. We run simulations separately for each number of trimers and aggregate the results. The rate of binding and unbinding

between Ab and mucin is given by rates m_{on} and m_{off} , respectively, and is assumed to be much larger than Ab-virion binding rates. It is assumed that the number of binding sites on mucin far exceeds the number of antibodies, and thus we can treat the Ab-mucin binding as a unimolecular reaction with respect to the Ab concentration.

Wide diffusivity variations between mucin, virions, and antibodies cause different binding characteristics to exist in certain cases. Antibodies bound to mucin are stationary and due to steric effects bind to virions at a reduced rate k_{on}^{b} given by the Smoluchowski encounter relation: $k_{\text{on}}^{\text{b}} = \frac{D_{\text{vir}}}{D_{\text{Ab}} + D_{\text{vir}}} k_{\text{on}}$. Similarly, antibodies bound to a free virion is less free to bind to mucin. This first binding reaction between an antibody bound only to a free virion and mucin is given by $m_{\text{on}}^{\text{first}} = \frac{D_{\text{vir}}}{D_{\text{Ab}}} m_{\text{on}}$. We assume all other binding reactions occur as if it were between free particles.

Given data that suggests that the rate of mucin and Ab reaction far exceeds that of Ab and virion reaction, we make an asymptotic assumption; we assume that the rate of binding and unbinding between mucin and antibodies is infinitely large and define the ratio $\alpha = \lim_{m_{\text{on}}, m_{\text{off}} \rightarrow \infty} \frac{m_{\text{off}}}{m_{\text{on}} + m_{\text{off}}}$ [3]. This dimensionless constant then defines the percentage of antibodies that are unbound from mucin at any temporal and spatial position. We can further show that the fraction of virions with n antibodies bound to it are trapped in the mucin by the ratio $\beta(n) = \frac{\alpha^n}{\alpha^n + R(1 - \alpha^n)}$, where $R = \frac{D_{\text{vir}}}{D_{\text{vir}} + D_{\text{Ab}}}$.

Advection is caused by a difference in osmolarity between the CVM and semen layer, causing a movement of fluid towards the cell layer. Because semen is not replenished during this process, fluid is permanently lost from the semen side and must be accounted for at the boundary. This is discussed further in the numerical approximation to the solution.

Given the radial symmetry in the cylindrical geometry, we model the system using a 1-D PDE where $x = 0$ symbolizes the cell layer and $x = L$ symbolizes the semen/air interface. The model is run for a particular location along the height of the cylinder (i.e. the z direction), which determines drainage properties as described later. With the addition of advection into the model, the movement and reactions between antibodies (u) and virions (v) can be described with the following initial boundary value problem derived from Fick's Second Law:

$$\frac{\partial}{\partial t} u(x, t) = \frac{\partial}{\partial x} \left(D_{\text{Ab}}^{\text{eff}}(x) \frac{\partial}{\partial x} u \right) - \frac{\partial}{\partial x} \left(V_{\text{Ab}}^{\text{eff}}(x) u \right) \quad (1a)$$

$$\begin{aligned} \frac{\partial}{\partial t} v(n, x, t) &= \frac{\partial}{\partial x} \left(D_{\text{vir}}^{\text{eff}}(n, x) \frac{\partial}{\partial x} v \right) - \frac{\partial}{\partial x} \left(V_{\text{vir}}^{\text{eff}}(x) v \right) \\ &+ (n + 1) k_{\text{off}} v(n + 1, x, t) + (3N^* - n + 1) \left(k_{\text{on}} u^{\text{free}}(x, t) + k_{\text{on}}^{\text{b}} u^{\text{bound}}(x, t) \right) v(n - 1, x, t) \\ &- n k_{\text{off}} v(n, x, t) - (3N^* - n) \left(k_{\text{on}} u^{\text{free}}(x, t) + k_{\text{on}}^{\text{b}} u^{\text{bound}}(x, t) \right) v(n, x, t) \end{aligned} \quad (1b)$$

$$\frac{\partial}{\partial x} u \Big|_{x=0} = 0, \quad t \geq 0 \quad (2a)$$

$$\frac{\partial}{\partial x} u \Big|_{x=L} = 0, \quad t \geq 0 \quad (2b)$$

$$v(n, 0, t) = 0, \quad t \geq 0 \quad (2c)$$

$$\frac{\partial}{\partial x} v \Big|_{x=L} = 0, \quad t \geq 0 \quad (2d)$$

$$u(x, 0) = \begin{cases} u_0, & 0 \leq x \leq 50 \\ 0, & 50 < x \leq 250 \end{cases} \quad (3a)$$

$$v(n, x, 0) = \begin{cases} 0, & 0 \leq x \leq 50 \\ v_0 \delta_{n,0} P((X \sim \text{NB}(\frac{28}{5}, \frac{5}{7})) = N^*), & 50 < x \leq 250 \end{cases} \quad (3b)$$

where $u(x, t)$ is the concentration of antibodies and $v(n, x, t)$ is the concentration of virions with n motors attached (assume $v(-1, x, t) = v(3N^* + 1, x, t) = 0$). The diffusive and advective coefficients are given by:

$$D_{\text{Ab}}^{\text{eff}}(x) = \begin{cases} \alpha D_{\text{Ab}}, & 0 \leq x \leq 50 \\ D_{\text{Ab}}, & 50 < x \leq 250 \end{cases} \quad (4a)$$

$$D_{\text{vir}}^{\text{eff}}(n, x) = \begin{cases} \beta(n) D_{\text{vir}}, & 0 \leq x \leq 50 \\ D_{\text{vir}}, & 50 < x \leq 250 \end{cases} \quad (4b)$$

$$V_{\text{Ab}}^{\text{eff}}(x) = \begin{cases} \alpha v_{\text{trans}}, & 0 \leq x \leq 50 \\ v_{\text{trans}}, & 50 < x \leq 250 \end{cases} \quad (5a)$$

$$V_{\text{vir}}^{\text{eff}}(n, x) = \begin{cases} \beta(n) v_{\text{trans}}, & 0 \leq x \leq 50 \\ v_{\text{trans}}, & 50 < x \leq 250 \end{cases} \quad (5b)$$

where v_{trans} is defined within the following subsections. The equations for virion movement given by Eq. 1b can be condensed to a compact form:

$$\frac{\partial}{\partial t} \vec{v}(x, t) = \frac{\partial}{\partial x} \left(\mathbf{D}(x) \frac{\partial}{\partial x} \vec{v} \right) - \frac{\partial}{\partial x} \left(\mathbf{V}(x) \vec{v} \right) + (f - g) \vec{v} \quad (6)$$

where $\mathbf{D}(x)$ is a $3N^* + 1 \times 3N^* + 1$ diagonal matrix with entries $D_{\text{vir}}^{\text{eff}}(n, x)$, $\mathbf{V}(x)$ is a $3N^* + 1 \times 3N^* + 1$ diagonal matrix with entries $V_{\text{vir}}^{\text{eff}}(n, x)$, and the components of the $3N^* + 1$ vector \vec{v} are $v_i = v(i, x, t)$.

This project seeks to understand the relative impact of the Ab binding characteristics on the prevention of HIV given these additions to the system. We define *infectivity* as the sum of the free trimers present on the virions that penetrate the cell layer, and seek to minimize this quantity over the lifetime of the system, which we simulate to run for 2 h.

2.2.1 Numerical Approximation to Solution

The PDEs described in Eq. 1a and 6 are solved numerically via a Forward-Time Centered-Space (FTCS) scheme. To compute the solution, the domain is divided into N regions of spatial size dx and T regions temporal size dt . By manipulation of Taylor Expansions about each spatial point, we can construct numerical approximation to each derivative. Defining $u_i^k = u(idx, kdt)$ and solving for u_i^{k+1} , we get the following for $1 \leq i \leq N - 3$:

$$u_i^{k+1} = u_i^k + \frac{dt}{dx^2} \left(D_{Ab}^{eff}((i+1)dx)u_{i+1}^k - 2D_{Ab}^{eff}(idx)u_i^k + D_{Ab}^{eff}((i-1)dx)u_{i-1}^k \right) - \frac{dt}{dx} \left(V_{Ab}^{eff}((i+1)dx)u_{i+1}^k - V_{Ab}^{eff}(idx)u_i^k \right) \quad (7)$$

Where, in order to maintain scheme stability throughout the entire system, we require that:

$$dt < \frac{dx^2}{2D_{Ab}} \quad (8)$$

Similarly for virions:

$$\bar{v}_i^{k+1} = \bar{v}_i^k + \frac{dt}{dx^2} \left(\mathbf{D}((i+1)dx)\bar{v}_{i+1}^k - 2\mathbf{D}(idx)\bar{v}_i^k + \mathbf{D}((i-1)dx)\bar{v}_{i-1}^k \right) - \frac{dt}{dx} \left(\mathbf{V}((i+1)dx)\bar{v}_{i+1}^k - \mathbf{V}(idx)\bar{v}_i^k \right) + dt(f-g)\bar{v}_i^k \quad (9)$$

Eq. 7 and 9 can also be applied to the cell layer/CVM boundary if the following constraints are applied based on the boundary conditions in Eq. 2a and 2c: $u_{-1}^n = u_0^n$ and $v_{-1}^n = 0$.

Because of the movement of fluid from the semen to the cell layer and the lack of a replenishing source, the boundary at the semen/air interface shrinks towards the cell layer at rate v_{trans} . To account for this, we adjust the spatial partition at the boundary such that the last two regions ($i = N - 1$ and $i = N$) are combined and possess a size of dx_{sem} . At $t = 0$, $dx_{sem} = 2dx$. At each time step, the size of the last cell i decreases by $v_{trans}dt$. In the iteration where $dx_{sem} \leq dx$, we incorporate the $(i - 1)^{th}$ spatial partition to the boundary and readjust the concentration as necessary.

To account for a different spatial step size in the system, the FTCS scheme must be adjusted at the last two spatial positions. First, note that because we are examining a scenario in the semen layer, we can reduce the diffusive and advective coefficients to their relevant constants in semen. Let $u_z^k = u((N-2)dx, kdt)$ and $u_{z+1}^k = u((N-2)dx + dx_{sem}, kdt)$. To compute the approximation for Ab, we use a sum of second order Taylor expansions of u about spatial locations $z - 1$ and z to calculate an approximation to the first and second derivatives to yield the solution at $(N - 2)dx$:

$$u_z^{k+1} = u_z^k + \frac{dtD_{Ab}}{dx^2dx_{sem} + dx_{sem}^2dx} \left(dx_{sem}u_{z-1}^k - (dx + dx_{sem})u_z^k + dxu_{z+1}^k \right) + \frac{v_{trans}}{dx_{sem}} \left(u_{z+1}^k - u_z^k \right) \quad (10)$$

For the solution at $(N - 2)dx + dx_{sem}$, we create the following constraints based on the reflective boundary boundary condition in Eq. 2b: $u_{N+1}^k = u_{z+1}^k$

$$u_{z+1}^{k+1} = u_z^k + \frac{dtD_{\text{Ab}}}{dx dx_{\text{sem}} + dx_{\text{sem}}^2} \left(u_z^k - u_{z+1}^k \right) - \frac{v_{\text{trans}}}{dx_{\text{sem}}} u_{z+1}^k \quad (11)$$

By performing the same operations on 6 with the boundary condition given by Eq. 2d, we get the same set of boundary equations:

$$\begin{aligned} \vec{v}_z^{k+1} = \vec{v}_z^k + \frac{dtD_{\text{vir}}}{dx^2 dx_{\text{sem}} + dx_{\text{sem}}^2 dx} \left(dx_{\text{sem}} \vec{v}_{z-1}^k - (dx + dx_{\text{sem}}) \vec{v}_z^k + dx \vec{v}_{z+1}^k \right) \\ + \frac{v_{\text{trans}}}{dx_{\text{sem}}} \left(\vec{v}_{z+1}^k - \vec{v}_z^k \right) + dt(f - g) \vec{v}_i^k \end{aligned} \quad (12)$$

$$\vec{v}_{z+1}^{k+1} = \vec{v}_z^k + \frac{dtD_{\text{vir}}}{dx dx_{\text{sem}} + dx_{\text{sem}}^2} \left(\vec{v}_z^k - \vec{v}_{z+1}^k \right) - \frac{v_{\text{trans}}}{dx_{\text{sem}}} \vec{v}_{z+1}^k + dt(f - g) \vec{v}_i^k \quad (13)$$

These solutions are computed in MATLAB using a grid size of $dx = 1$. After each simulation, the average infectivity of virions that pass through the cell layer is calculated and stored. The next sections describe the exact setup of the system and analysis of the PDE solutions.

2.3 Transport Scaling Analysis

Our first investigation dealt with the addition of the advective term to the system. For the purposes of our initial analysis, we refrain from using an experimental value of v_{trans} and instead define the following relation via the definition of the Peclet Number:

$$v_{\text{trans}} = Pe \frac{D_{\text{vir}}}{L} \quad (14)$$

where when $0 \leq Pe < 1$, the system will be primarily dominated by diffusion. We are particularly interested in studying the effect of virion penetration as a result of advection. In this simplified model, the pressure difference is assumed to exist at a fixed value throughout the simulation, such that the advective speed v_{trans} is a constant with respect to both space and time.

All other parameters are kept constant and the infectivity is determined as a function of the Peclet number. This is compared to the infectivity when $Pe = 0$. Figure 1 shows the results. The two curves plotted describe the upper and lower bound of infectivity (as given in a previous work [11]). We see that there is not a significant increase in infectivity until Pe approaches or exceeds 1. Pe must exceed 0.5 before the infectivity increases by 10%. As we would expect, once the system becomes advection dominated (when $Pe > 1$), the infectivity increases at a seemingly exponential rate. We also see that there is a fairly small margin between the relative infectivities when α changes. Although the difference is small, the relative increase is higher in cases with no trapping ($\alpha = 1$). This gives an upper bound to the effect of pressure-driven advection on the entire system.

With an implementation and general understanding of the effect of transport on infectivity, we next seek to add the relevant physiological constraints and determine the net effect on infection potential.

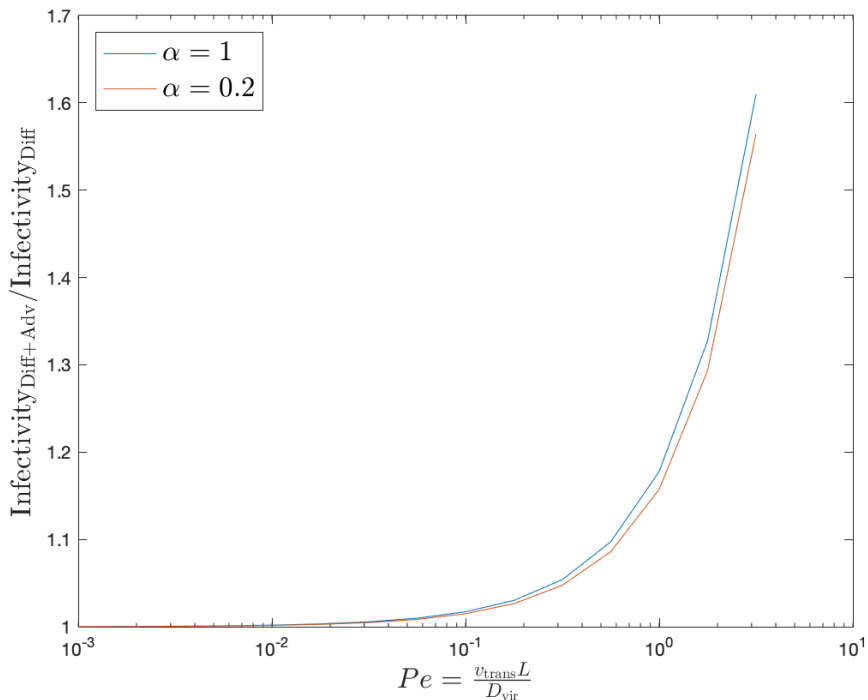


Figure 1: Relative change in virion infectivity

2.4 Virion Infectivity

We next move to a more physiologically relevant study of the effects of transport and drainage on the system. Advection is caused by the flow of fluid into the CVM and cell layer. As mentioned in the discussion of the boundary conditions above, semen is not replenished in this system, and as such the difference in pressure is quickly eliminated (in approximately 15 minutes). By Darcy's Law, the change in fluid pressure M can be described by the following ODE:

$$v_{\text{trans}}(t) = \frac{\partial}{\partial t} M_{\text{sem}} = k(M_{\text{CVM}} - M_{\text{sem}}) \quad (15)$$

For the purpose of numerical calculations, we assume the condition that at $t = 900$ s, $|M_{\text{sem}} - M_{\text{CVM}}| < 0.5$. Thus, we can solve the ODE and calculate the rate constant to be $k = \frac{-\ln(0.5/(M_{\text{sem}}(0) - M_{\text{CVM}}))}{900}$. Thus:

$$v_{\text{trans}}(t) = \begin{cases} \frac{-\ln(0.5/(M_{\text{sem}}(0) - M_{\text{CVM}}))}{900} (M_{\text{sem}}(t) - M_{\text{CVM}}), & 0 \leq t \leq 900 \text{ s} \\ 0, & t > 900 \text{ s} \end{cases} \quad (16)$$

Because Fick's Law is independent of time on the right hand side, the conversion of v_{trans} from a constant to a function of time does not affect any prior work. Also, by the same solution, we see that $M_{\text{sem}}(t)$ decreases to the CVM osmolarity in an exponential fashion. We vary the value of $M_{\text{sem}}(0)$ to adjust the magnitude of the advective push. Using a minimum physiological value of $M_{\text{sem}}(0) = 320$ and normal value of $M_{\text{CVM}} = 380$, we get

an initial velocity of $v_{\text{trans}}(0) = 0.32 \mu\text{m s}^{-1}$, which corresponds to $Pe = 63$. However, this quantity also decreases exponentially to 0 after 900 s. Thus, the initial expectation is that the addition of advection will affect the overall infectivity.

The next major physiological phenomenon is the drainage of semen out of the vagina over time. Over the span of approximately 5 minutes shortly after deposition, semen is liquefied and removed from the system by a variety of mechanical processes. As such, this process removes a considerable number of virions from the system. This process is modeled via a so-called "escalator model", where semen that leaves from the introitus is quickly replaced by semen directly above, causing a net loss at the cervical side of the semen first. Again, this also has implications on the boundary condition at the semen/air interface. We vary the parameters ρ , the fraction of semen drained in total and t_{drain} , the time that drainage begins to take effect, examine the effects on the system.

We remove semen from the system due to drainage in a discrete fashion. Based on the position along the vaginal canal the model is run, ρ , and a drainage span of 5 minutes, we calculate the time that spatial partition i is removed from the system. When this occurs, we readjust the boundary position again such that the size of the final cell remains dx_{sem} .

With the addition of the numerical components, we next move to computing solutions over our parameter space to determine optimum trapping scenarios and the effect of the additions on this optimum. We first study the effect of drainage on the system. Intuitively, we would expect that as the amount of semen increases, the total number of virions in the system will decrease and thus the total flux across the cell layer will also decrease.

Figure 2 plots the total flux virion flux across the cell layer. While we see a monotonic decrease in flux, we also see that in all setups, a low drainage ($< 50\%$) results in a nearly negligible decrease in flux. Most of the semen must be drained early in the simulation before there is a clear change in flux. This is because flux attains its highest rate in the beginning of the model and consists mostly of virions with few antibodies attached and starting close to the CVM boundary. Drainage would be unable to influence the penetration of virions that have already travelled into the CVM, and would have a modest effect on those that are close to the interface.

Another affect of drainage is the changes that would arise between different locations along the vagina. Figure 3 shows the number of virions that enter the cell layer at different locations in the modeled cylinder. We see that the number of virions that enter the cell layer is essentially constant over the entire stack when drainage is in place. Again, we see that drainage does not play a significant role in varying the behavior of the model. From this point on, we simplify the model to only solve at the cervix ($z = 0 \mu\text{m}$).

Next, we study the effect of advection on the system. Figure 4 shows that, relative to drainage, osmolarity difference has a more dramatic and sustained effect on flux. The push of particles towards the cell layer makes the effective distance shorter for virions, even if advection ends shortly after the beginning of the system. It is interesting to note that for small differences in osmolarity, the flux seems to decrease in some cases. One potential theory is that because antibodies also experience advection, the push away from the semen/air interface prevents antibodies from being drained away, However, this effect is very quickly overcome as the osmolarity difference increases.

Finally, given some characteristic values for drainage and osmolarity difference, we seek to identify the binding affinity between Ab and mucin that best maximizes trapping. Figure 5

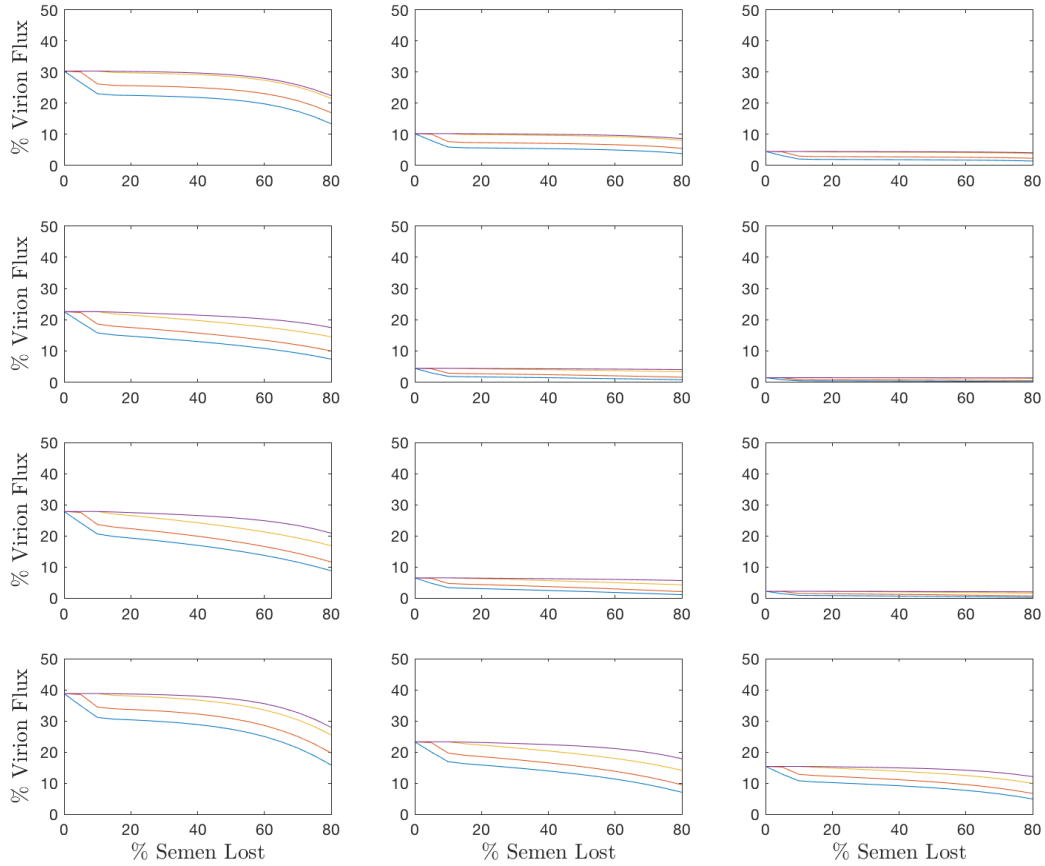


Figure 2: Total virion flux over varying levels of drainage. Each row is for a particular α value (from top to bottom: 0.02, 0.3, 0.5, and 0.8). Each column is a particular antibody concentration (from left to right, 1, 5, and 10). The colored curves represent different drainage times (blue = 0 min, orange = 1 min, yellow = 5 min, purple = 10 min)

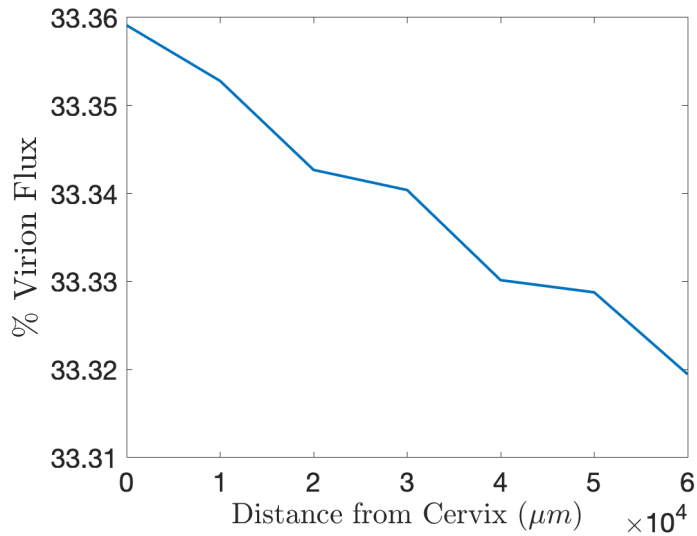


Figure 3: Total virion flux at different positions along the vagina. Parameters used are: drain % = 50 % and drain start time = 5 min.

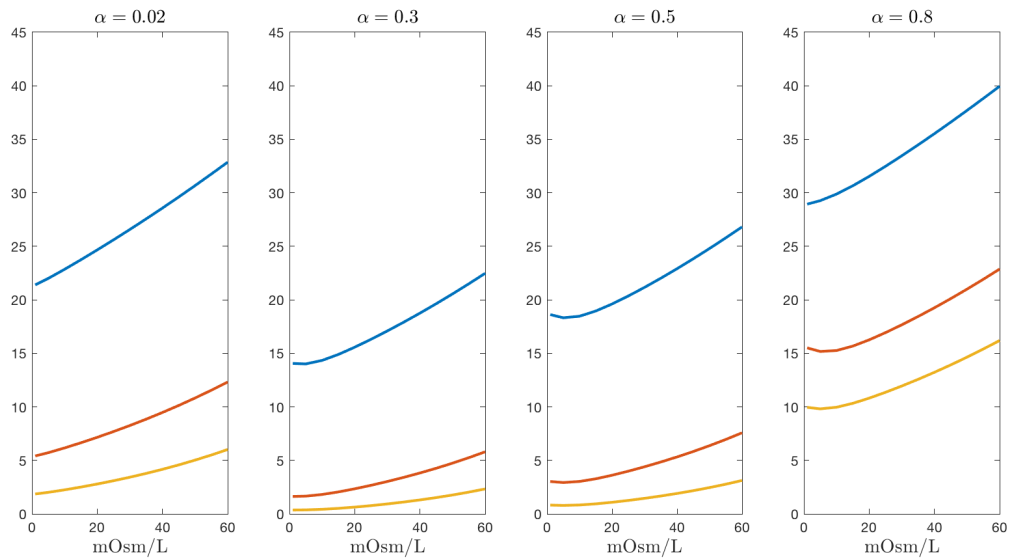


Figure 4: Total virion flux over varying beginning osmolarities. Each panel is a particular α value (from left to right, 0.02, 0.3, 0.5, and 0.8). Each curve is a particular antibody concentration (blue = 1, orange = 5, yellow = 10).

shows the results. The top two figures show a competing effect that α (Ab-mucin affinity) has on the profiles of virions that enter the body. The top left image shows that in general, a low α (i.e. high affinity between Ab and mucin) decreases the number of virions that enter the body. However, the top right image shows that virions that penetrate in a low α system have a high average infectivity; a high value of α is necessary to decrease the infectivity of a single virion.

These competing effects create a minimum in the overall infectivity around $0.2 < \alpha < 0.4$, as seen in the bottom right figure. And as we would expect, as more Ab are present in the system, overall trapping improves dramatically. Thus, we can again conclude that optimum antibody characteristics are to have a modest affinity to mucin polymers. The addition of transport and drainage, while overall more detrimental to the potential protection afforded by antibodies, does not significantly influence the optimum Ab binding characteristics.

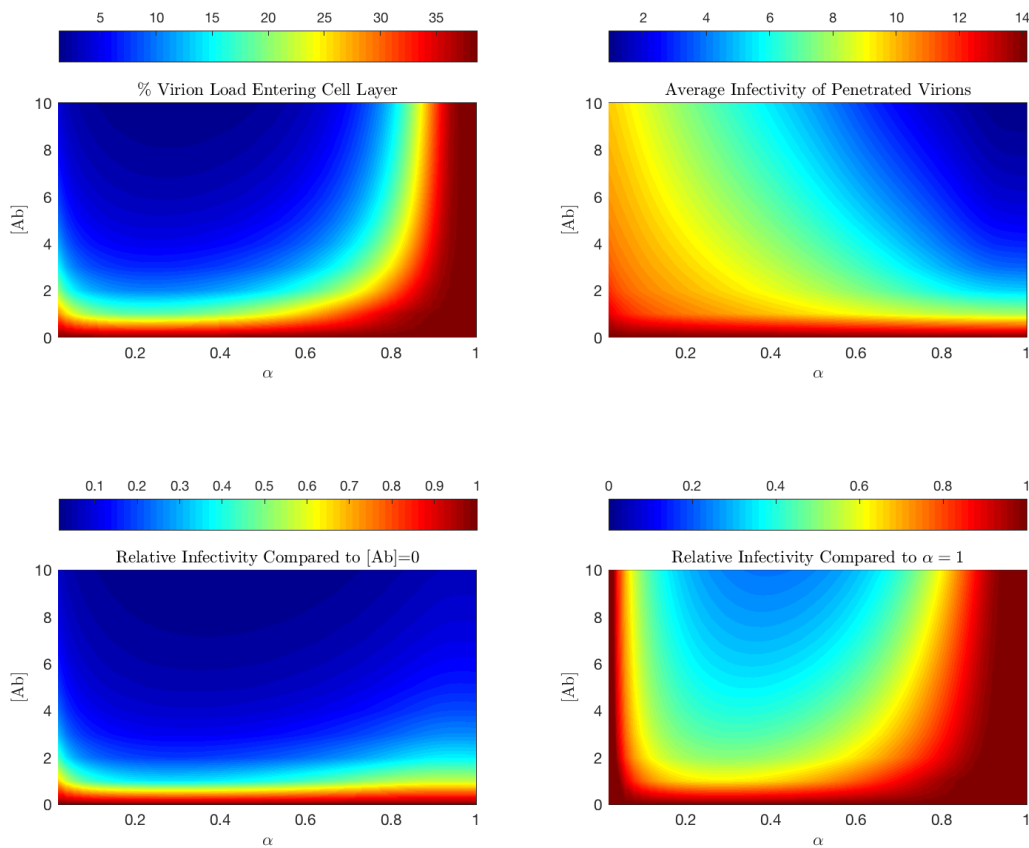


Figure 5: Profile of penetrating virions for certain Ab characteristics. Values used are: $M_{\text{sem}}(0) = 340$, $M_{\text{CVM}} = 380$, drain % = 50 %, drain start time = 5 min.

3 Multi-Scale Model of Axonal Transport

3.1 Background

The following section is a discussion on much of the same mathematical principles used in Section 2 but in a different biological system. Within most cells exists a scaffolding network of polymers known as microtubules (MT) that performs many structural functions from maintaining cell shape to cell division. They are also essential means of transporting molecular materials between various parts of the cell. This is especially important in cells like neurons, which require materials (like neurotransmitters) to be sent away from the soma (where most proteins are manufactured) down the axon, marked by extremely long distances and branches [1].

The makeup of the packaged materials (called "cargo" in this work) varies widely. Various proteins and nucleic acids can be transported, as well as larger structures like mitochondria. Movement down the MT is facilitated by molecular motor proteins. These proteins are generally "Y" shaped, with the base of the Y attaching to the cargo and the two forks binding and unbinding to the MT. One particular protein, kinesin, generally travels away from the soma due to the polarized nature of the MT. While many proposed mechanisms for the movement of kinesin have been discussed, it is known that kinesin operates by binding and unbinding each head rapidly to the MT, and using ATP as an energy source to take "steps" down with cargo [5].

The movement of kinesin can thus be thought of as a stochastic process, where kinesin waits until a binding or unbinding event to continue to the next phase in the cycle. It is also common for the kinesin to detach from the MT during transport. Kinesin that have detached are then forced to diffuse (along with any cargo it is attached to) until it can find a new MT. Despite a single motor's low processivity, the overall efficiency of this system remains high. One likely cause is the ability for multiple motors to act on a given cargo [6]. This way, if one motor unbinds from the MT, there are other motors available to drive transport [7]. However, it is still unclear why this system would be preferred to using single motors with a high affinity for MT. This section describes a model for kinesin transport along MT and seeks to identify the optimum binding characteristics between motors and MT. We use both a probabilistic and deterministic model to examine the efficiency of the system for a given set of physiological parameters. This work was conducted directly under Dr. Jay Newby (University of Alberta) based on the work presented in Section 2 along with a more general framework for Ab trapping in mucus [9].

3.2 Model

For the purpose of this work, an axon is modeled as a 1-D line with an even distribution of motor/MT binding sites throughout. Kinesin motors are assumed to be uniformly distributed throughout the system at a concentration much higher than that of cargo, and thus there are no depletion effects. All cargo begin at $x = 0$ and have no motors bound to it.

Like the Antibody/Virion model described in the previous section, motors act much like antibodies, cargo act like virions, and the MT act like mucin polymers. Motors and cargo diffuse with constants D_{motor} and D_{cargo} respectively. A motor binds and unbinds from a

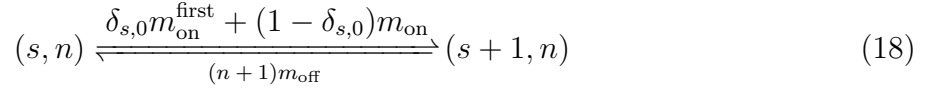
microtubule at a rates m_{on} and m_{off} respectively. Cargo bind and unbind from motors at various rate k_{on} and k_{off} respectively. We use the same constant $\alpha = \frac{m_{\text{off}}}{m_{\text{off}} + m_{\text{on}}}$ to describe the rate of binding and unbinding of motor and microtubules. Motors bound to MT are less able to bind to cargo because of steric hinderances, and thus the reduced binding rate is given by $k_{\text{on}}^{\text{b}} = \frac{D_{\text{cargo}}}{D_{\text{cargo}} + D_{\text{motor}}} k_{\text{on}}$. Similarly for a motor bound to a cargo that is freely diffusing, the reduced binding rate for the first motor is $m_{\text{on}}^{\text{first}} = \frac{D_{\text{cargo}}}{D_{\text{motor}}} m_{\text{on}}$. When unbounded, motors and cargo move freely through diffusion. When bounded, motors (with cargo) move at a constant velocity along the microtubule.

Experimental parameters for binding, transport, and diffusion motivates the following timescale separations:

$$\tau_{\alpha} \ll \tau_K < \tau_v < \tau_D, \quad (17)$$

where $\tau_{\alpha} = \frac{1}{m_{\text{on}} + m_{\text{off}}}$ is the timescale of binding between motors and MT, $\tau_K = \frac{1}{k_{\text{on}} + k_{\text{off}}}$ is the timescale of binding between motors and cargo, $\tau_v = \frac{L}{v_{\text{trans}}}$ is the timescale of cargo transport, and $\tau_D = \frac{x^2}{2D_{\text{cargo}}}$ is the timescale of cargo diffusion.

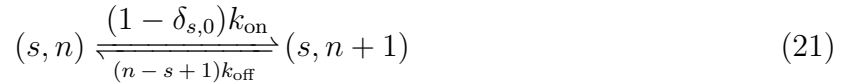
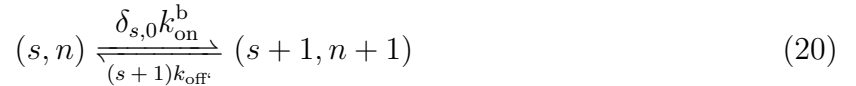
The motor/MT binding reactions can be modeled with the following state change:



which motivates the following rate matrix:

$$M_s = \begin{bmatrix} -n \frac{D_{\text{cargo}}}{D_{\text{motor}}} m_{\text{on}} & m_{\text{off}} & 0 & 0 & \dots & 0 \\ n \frac{D_{\text{cargo}}}{D_{\text{motor}}} m_{\text{on}} & -(n-1)m_{\text{on}} - m_{\text{off}} & 2m_{\text{off}} & 0 & \dots & 0 \\ 0 & (n-1)m_{\text{on}} & -(n-2)m_{\text{on}} - 2m_{\text{off}} & 3m_{\text{off}} & \dots & 0 \\ \vdots & \vdots & \vdots & \ddots & \vdots & \vdots \\ 0 & 0 & 0 & \dots & \dots & -nm_{\text{off}} \end{bmatrix} \quad (19)$$

Similarly for motor/cargo binding reactions:



and the following rate matrix:

$$V_{n,s} = \begin{bmatrix} -N(k_{\text{on}} + k_{\text{on}}^b) & k_{\text{off}} & 0 & \dots & 0 \\ N(k_{\text{on}} + k_{\text{on}}^b) & -k_{\text{off}} - (N-1)(k_{\text{on}} + \delta_{s,0}k_{\text{on}}^b) & 2k_{\text{off}} & \dots & 0 \\ 0 & (N-1)(k_{\text{on}} + \delta_{s,0}k_{\text{on}}^b) & -2k_{\text{off}} - (N-2)(k_{\text{on}} + \delta_{s,0}k_{\text{on}}^b) & \dots & 0 \\ 0 & 0 & (N-2)(k_{\text{on}} + \delta_{s,0}k_{\text{on}}^b) & \ddots & 0 \\ 0 & 0 & 0 & & 0 \\ \vdots & \vdots & \vdots & & nk_{\text{off}} \\ 0 & 0 & 0 & & -nk_{\text{off}} \end{bmatrix} \quad (22)$$

3.2.1 QSS Reduction of the CK Equation

In this section we use the asymptotic binding assumption used in the Ab/virion model to arrive at the PDE under steady-state binding conditions.

We begin our analysis with the Chapman-Kolmogorov master equation:

$$\frac{\partial}{\partial t} p(n, s, x, t) = \delta_{s,0} D_{\text{cargo}} \frac{\partial^2 p}{\partial x^2} - (1 - \delta_{s,0}) v_{\text{trans}} \frac{\partial p}{\partial x} + \sum_{i=0}^N [M_s]_{s,i} p(n, i, x, t) + \sum_{i=0}^N [V_{n,s}]_{n,i} p(i, s, x, t) \quad (23)$$

where $p(n, s, x, t)$ is a probability density function describing cargo position at spatial position x , time t .

The initial condition is given by

$$p(n, s, x, 0) = \delta_{n,0} \delta_{s,0} \delta(x). \quad (24)$$

We will consider two sets of boundary conditions: periodic

$$p(n, s, 0, t) = p(n, s, L, t), \quad \frac{\partial}{\partial x} p(n, s, 0, t) = \frac{\partial}{\partial x} p(n, s, L, t), \quad (25)$$

and right-end absorbing

$$p(n, s, L, t) = 0. \quad (26)$$

Using our timescale separations, we can assume that the system will be at steady state with respect to binding from $t \geq 0$. Thus, we can approximate the binding reactions as independent and state that $p(n, s, x, t) \approx \pi_\alpha(s|n) \pi_K(n) u(x, t)$, where u is the normalized concentration of cargo at position x and time t . π_α and π_K are the stationary distributions of the Markov processes given by M_s and $V_{n,s}$. Each matrix describes an irreducible, aperiodic Markov chain, and thus we can solve for the (unique) stationary distributions by solving $V_{n,s} \vec{\pi}_\alpha = 0$ and $M_n \vec{\pi}_K = 0$. Using the asymptotic approximation $\alpha = \lim_{m_{\text{on}}, m_{\text{off}} \rightarrow \infty} \frac{m_{\text{off}}}{m_{\text{on}} + m_{\text{off}}}$, the system results in the following probability distributions:

$$\pi_\alpha(s|n) = \begin{cases} \frac{D_{\text{motor}} \alpha^n}{(D_{\text{motor}} - D_{\text{cargo}}) \alpha^n + D_{\text{cargo}}}, & s = 0 \\ \frac{\binom{n}{s} D_{\text{cargo}} \alpha^{n-s} (1-\alpha)^s}{(D_{\text{motor}} - D_{\text{cargo}}) \alpha^n + D_{\text{cargo}}}, & s \neq 0 \end{cases} \quad (27)$$

$$\pi_K(n) = \frac{\mathcal{N}}{k_{\text{off}}^n} \prod_{j=0}^{n-1} (\pi_\alpha(0|n)k_{\text{on}} + k_{\text{on}}^b) \quad (28)$$

where \mathcal{N} is a normalization constant. By applying our approximation to the full probability density to 23 and summing across all values of s and n , we remove the dependence on the current binding state and get the following PDE:

$$\frac{\partial}{\partial t} u(x, t) = \bar{D} \frac{\partial^2}{\partial x^2} u - \bar{v} \frac{\partial}{\partial x} u, \quad (29)$$

where

$$\bar{D} = D_{\text{cargo}} \sum_{n=0}^N \pi_\alpha(0|n) \pi_K(n), \quad \bar{v} = v_{\text{trans}} \sum_{n=0}^N \sum_{s=1}^n \pi_\alpha(s|n) \pi_K(n). \quad (30)$$

The reduced parameters, \bar{D} and \bar{v} , are the steady-state diffusivity and transport velocity respectively of a population of cargo.

3.2.2 Analytic and Numerical Solutions

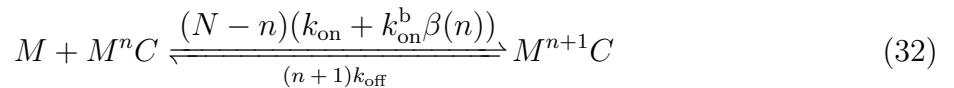
In this work, we take two approaches to analyzing the molecular motor system. The first is an analytic approximation to the advection-diffusion equation given by Eq. 29. The second is a numerical simulation of the partial QSS reduced system.

We will first focus our attention on the first approach, which we will consider for only the Robin boundary condition IBVP. Eq. 29 can be easily solved over the entire real line using the Fourier Transform method to yield a gaussian. To account for the boundary conditions, we utilize the Method of Images over the absorbing boundary to truncate the domain to $(-\infty, L]$. This yields the closed-form approximation:

$$u(x, t) = \frac{1}{\sqrt{4\pi\bar{D}t}} \left(e^{-\frac{(x-\bar{v}t)^2}{4\bar{D}t}} - e^{\frac{\bar{v}L}{\bar{D}} - \frac{(x-\bar{v}t-2L)^2}{4\bar{D}t}} \right). \quad (31)$$

To prevent a buildup of an infinite series, we only consider this solution over the domain $[0, L]$. This inherently produces error that will be discussed later.

We now examine the second approach, which works for either boundary condition considered. Under a partial QSS assumption, we assume an asymptotic binding rate for only the motor/MT binding rates. This allows us to condense the system of two binding reactions to one effective binding reaction between motors and cargo. We define $\beta(n)$ as the probability that a cargo with n motors bound is free from the MT (i.e. the probability that $s = 0$). Based on the binding rates of motors to MT, the probability that a cargo with n motors is freely diffusing is given by $\beta(n) = \frac{\alpha^n}{\alpha^n + R(1-\alpha^n)}$, where $R = \frac{D_{\text{cargo}}}{D_{\text{cargo}} + D_{\text{motor}}}$. The effective binding and unbinding of a cargo and motor is summarized in Eq. 32:



Where M denotes a motor and C denotes a cargo. We use this binding reaction along with the diffusive and transport terms to define a one-dimensional partial differential equation given by Eq 33:

$$\frac{\partial}{\partial t} \vec{u}(x, t) = \mathbf{D} \frac{\partial^2}{\partial x^2} \vec{u} - \mathbf{V} \frac{\partial}{\partial x} \vec{u} + \mathbf{A} \vec{u} \quad (33)$$

where the vector u is an $N + 1$ vector of cargo concentrations and the i^{th} component corresponds to cargo with i motors bound. \mathbf{D} and \mathbf{V} are diagonal matrices with $\mathbf{D}_{ii} = \beta(i)D_{\text{cargo}}$ and $\mathbf{V}_{ii} = (1 - \beta(i))v_{\text{trans}}$. \mathbf{A} has values on the off-diagonals corresponding to the reactions in Eq 32. In this work, Eq 33 is solved in MATLAB and data is stored as concentrations and fluxes at each position and time. The Forward-Time Centered-Space method is used to solve to create the following numerical approximation:

$$\vec{u}_i^{k+1} = u_i^k + \frac{dt\beta(i)D_{\text{cargo}}}{dx^2} \left(\vec{u}_{i+1}^k - 2\vec{u}_i^k + \vec{u}_{i-1}^k \right) - \frac{dt(1 - \beta(i))v_{\text{trans}}}{dx} \left(\vec{u}_{i+1}^k - \vec{u}_i^k \right) + dt\mathbf{A}\vec{u}_i^k \quad (34)$$

The stop criterion is determined by the amount of cargo still in the system. For steady-state analyses we choose a periodic boundary condition and a uniformly distributed initial condition of cargo with $n = 0$. The stop criterion in this setup is determined by the magnitude of the change in the distribution of cargo concentrations with respect to n .

See Figure 6 for a comparison between the computational and analytic methods. The solution is best for large \bar{v} because the effect of the absorbing boundary condition at $x = 0$ is minimized. Therefore, for a given diffusivity and transport velocity, using the optimal α will create the best congruence between the two schemes. At worst (i.e. $\bar{v} = 0$), the analytic solution is half the value of the computational model for all x . Because the focus on this work was primarily on the agreement between the analytic and computational \bar{v} , performing a more exact calculation was not necessary. It is possible to perform additional iterations of the Method of Images to improve the analytic solution. This procedure can be done infinitely, creating a sequence of functions that converges to the same solution as the computational scheme (up to machine precision).

3.3 Kinetic Properties of System on Overall Transport

We first examine the role that binding between motors and cargo has on the overall transit times. We calculate the amount of time needed for half the cargo to reach the end of the system given the Robin boundary conditions (i.e., the median passage time; Figure 7(A)). Here, shorter median passage times correlate with an increase in the system's efficiency in moving cargo. At very small length scales (i.e. $< 1 \mu\text{m}$) where diffusion dominates (where $Pe = \frac{vL}{D_{\text{cargo}}} < 1$), faster binding results in longer transit times. As binding increases, cargo are more likely to be traveling down the MT and not diffusing. After approximately $2 \mu\text{m}$, we see the more expected conclusion that faster binding correlates with faster passage times. From the distribution of motors on cargo (as given by Figure 7(B)), we see that motors and cargo fairly quickly reach a steady state distribution, but have a very wide spread in the number of motors on cargo. Overall, the vast majority of cargo have multiple motors bound to it, as we would expect.

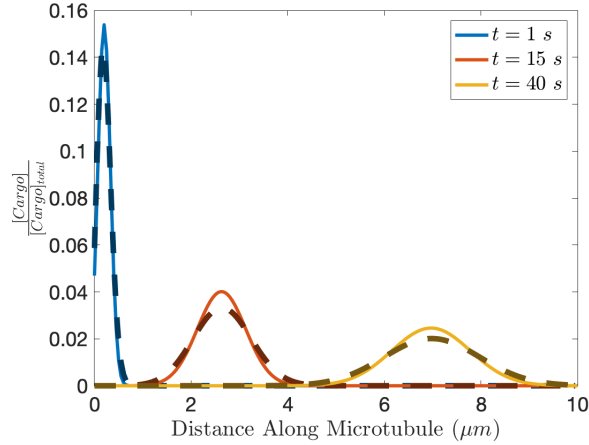


Figure 6: Comparison of Steady-state computational scheme and analytic scheme defined by Eq 31. Constants used: $N = 10$, $L = 10 \mu\text{m}$, $v_{\text{trans}} = 1 \mu\text{m s}^{-1}$, $k_{\text{on}} = .2 \text{ Hz}$, $k_{\text{off}} = 1 \text{ Hz}$, $D_{\text{cargo}} = .01 \mu\text{m}^2 \text{ s}^{-1}$, and $D_{\text{motor}} = 10 \mu\text{m}^2 \text{ s}^{-1}$

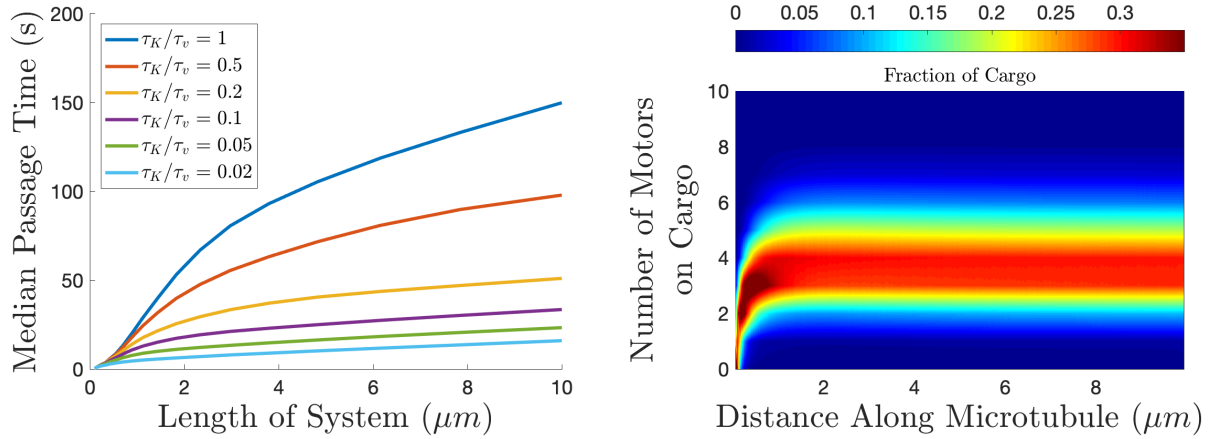


Figure 7: The effect of timescale separation on transport efficiency. (A) The median time to reach the end of the system. (B) The distribution of motors on the cargo (at the median time) as a function of distance along the MT. Constants used are: $N = 10$, $D_{\text{cargo}} = 0.014 \mu\text{m}^2 \text{ s}^{-1}$, $D_{\text{motor}} = 1.4 \mu\text{m}^2 \text{ s}^{-1}$, $v_{\text{trans}} = 1 \mu\text{m s}^{-1}$, $\alpha = 0.1$, $k_{\text{on}} = 5 \text{ Hz}$, $k_{\text{off}} = 1 \text{ Hz}$.

3.4 Maximization of Effective Transport

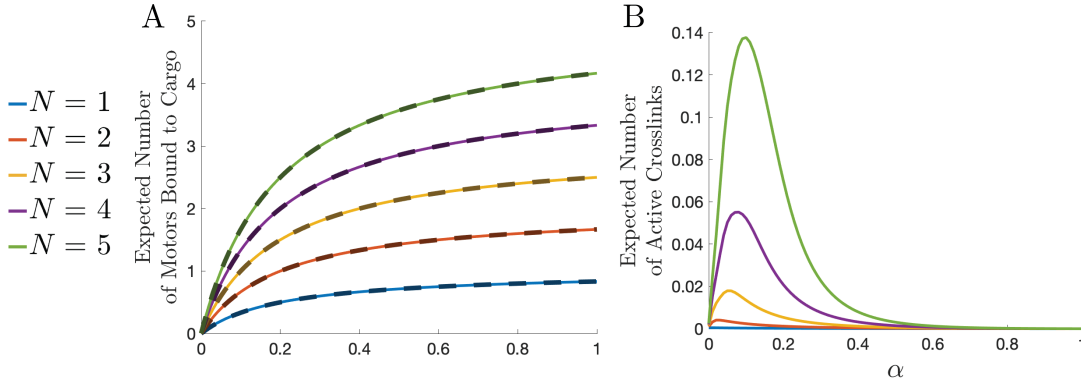


Figure 8: The average number of motors and average number of engaged motors at steady state. Solid lines denote the the QSS solution and dashed lines denote the computational solution. (A) Expected number of motors on cargo. (B) Expected number of motors bound to both cargo and MT. Other parameters used for both cases are: $L = 10 \mu\text{m}$, $v_{\text{trans}} = 1 \mu\text{m s}^{-1}$, $k_{\text{on}} = 5 \text{ Hz}$, $k_{\text{off}} = 1 \text{ Hz}$ and $D_{\text{motor}} = 1.4 \mu\text{m}^2 \text{s}^{-1}$.

We next look at the steady-state properties of transport down MT. Once motors and cargo have time to bind, the properties between the QSS and numerical solutions should match exactly, and thus in most locations they are plotted together. To understand the relationship between processivity and transport, we look at the average number of motors on the cargo. We now begin to use the periodic boundary condition and run until the distribution of motors on cargo approaches a steady-state distribution, and use this to calculate expected values. We also use the analytic equation for the conditional probability given by Eq 27 and 28 to calculate the expected number of crosslinks.

Much like the plots in Section 2, the optimum seen in Figure 8(B) for $N > 1$ is a result of two competing factors. Although more motors overall are bound to MT when $\alpha \rightarrow 0$, we see from Figure 8(A) that as α increases we get more motors on any given cargo because the encounter rate is higher between freely-diffusing motors and cargo.

We next calculate the expectation of the velocity at steady state to yield Figure 9(A). We see a significant change in transport flux with respect to α . From Figure 9(C) we see that the optimum appears around $\alpha = 0.1$ in most cases. Moreover, by increasing the total number of binding sites, we see that the optimum value of α increases. Thus, limited processivity leads to larger steady-state transport fluxes than infinite processivity, as long as cargo have more than one place to bind to motors. To see just how beneficial limited processivity is to transport of cargo, we calculate the percentage change in flux between $\alpha = 0$ and $\alpha = 0.1$ for different values of N and present it in Figure 9(B). We see here that the use of limited processivity increases the flux by as much as 300% when cargo are very large (i.e. have very small diffusivities).

Based on the preceding discussion, we conclude that cooperation among molecular motors robustly enhances transport flux, which can be further optimized by tuning processivity. However, motors must be allowed sufficient time to bind and accumulate on the cargo so that once the complex encounters a MT, many motors are able to cooperate during transport.

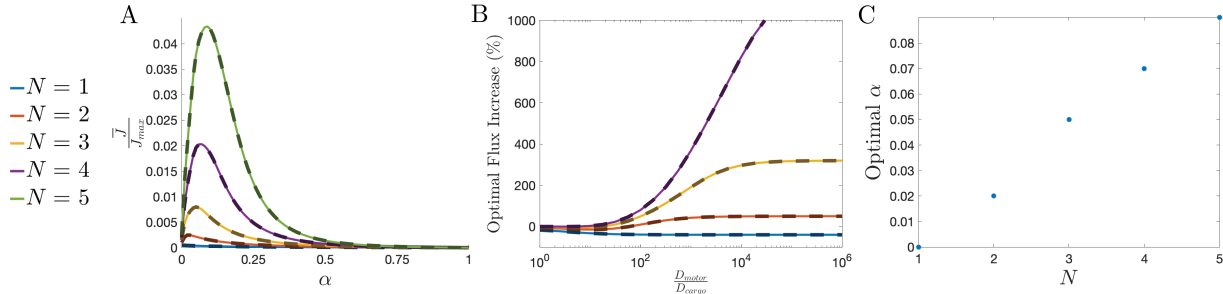


Figure 9: The steady state behavior as a function of α , the fraction of freely diffusing motors. (A) Effective transport flux, calculated using the velocity of the cargo population once net binding rate between cargo and motors reached 0 ($D_{cargo} = 0.14 \cdot 10^{-3} \mu\text{m}^2 \text{s}^{-1}$). (B) Maximum % increase in steady-state effective flux when motors are allowed to dissociate from MTs during transport. (C) α values at the peaks in (A) as a function of N . Solid lines denote the QSS solution and dashed lines denote the computational solution. Same parameter values as used in Figure 8.

4 Conclusion

This work explores a similar Reaction-Advection-Diffusion equation applied to two biological systems. The basis for analysis lies in the asymptotic approximation of binding applied by taking advantage of the clear timescale separations between binding and movement. This allows us to analyze our numerical simulations with a larger time step and simplify our analytical work while maintaining physiological relevance.

Work in the antibody/virion model shows the physiological robustness of antibody trapping with the addition of osmotic pressure gradients towards the cell layer. Because of the speed at which a pressure equilibrium is attained, the system remains diffusion-dominated for majority of the time and thus trapping of Ab to virions is still effective at preventing virions from penetrating to the cell layer. Additionally, trapping is optimized in regimes where Ab possess a weak affinity for mucin, which strengthens the claim made by the group in a previous work [11]. The molecular motor model shows again that allowing multiple motors on a cargo exponentially increases the probability of maintaining at least one motor engaged to the MT at all times. This is true for any fixed $0 < \alpha < 1$ (the fraction of freely diffusing motors). As motor processivity is increased ($\alpha \rightarrow 0$), there are many motors on MTs but very few on freely diffusing cargo. On the other hand, as $\alpha \rightarrow 1$, there are potentially many motors bound to a cargo, but few motors engaged to a MT. These competing factors set the stage for an optimal transport flux for an intermediate value of $0 < \alpha < 1$ (we observe $\alpha \approx 0.1$ is optimal for reasonable parameter choices).

We have also shown that cargo with smaller diffusivities (larger hydrodynamic radius) compared to individual motors benefit more from low-processivity motors than smaller cargoes with higher diffusivity. Because bimolecular binding rates are diffusion-dependent, smaller diffusivities lead to lower binding rates. The binding rate (k_{on}^b) between engaged motors (on a MT) and freely diffusing cargo is proportional to D_{cargo} . The binding rate (k_{on}) between freely diffusing motors and cargo is proportional to $D_{cargo} + D_{motor}$, which is comparatively unaffected by cargo size and diffusivity when $D_{cargo} \ll D_{motor}$. As a result,

motor-cargo binding at $\alpha = 0$ (where all motors are engaged to a MT) becomes an unlikely event for large cargoes with small diffusivity.

The common theme among these systems highlights a growing consensus among researchers in a variety of biological systems: weak binding among cooperative proteins maximizes the efficiency of these systems. Protein cooperation compounds their singular effects to form more effective complexes. In a simplified system where protein binding acting as a simple switch, adding multiple switches combines the probability of detaching in a multiplicative fashion. Thus, it is worth decreasing the affinity for a single protein so that they can perform other functions like diffusing throughout the system and increasing the number of proteins on a single target particle.

In the future, the antibody model will be used in conjunction with experimental *in vitro* data to further investigations on optimal antibody characteristics. As for the current model, incorporating variations in the fluid properties (i.e. viscosity) and large-scale mechanical dynamics (i.e. muscle contractions in the vaginal wall) will allow the model to move closer to an *in vivo* model. Recent work in the molecular motor model currently takes a stochastic view in conjunction with continuum processes to understand dynamics of certain processes like in traffic jams. Other considerations examining 3-D microtubule networks and branching geometries in axons can also lead to insights on how resources are transported to different areas of the cell and the responses to crowded environments.

5 Acknowledgements

I would like to thank Dr. Gregory Forest and Dr. Sam Lai for their allowing me to work in their group and explore research in mathematical biology. Their support and mentoring has helped me continue on in a path to academia. I would also like to thank Dr. Tim Wessler and Dr. Jay Newby for working closely with me and providing much needed direction throughout the course of our projects. Finally, I would like to thank my parents for their support in my academic and career goals throughout my time in school.

References

- [1] P. C. Bressloff and J. M. Newby. Stochastic models of intracellular transport. *Reviews of Modern Physics*, 85(1):135, 2013.
- [2] D. Burton and J. Mascola. Antibody responses to envelope glycoproteins in hiv-1 infection. *Nature Immunology*, 16(6):571–6, 2015.
- [3] A. Chen, S. McKinley, S. Wang, F. Shi, P. Mucha, M. Forest, and S. Lai. Transient antibody-mucin interactions produce a dynamic molecular shield against viral invasion. *Biophysical Journal*, 106(9):2028–36, 2014.
- [4] B. Corthesy. Role of secretory immunoglobulin a and secretory component in the protection of mucosal surfaces. *Future Microbiology*, 5(5):817–29, 2010.

- [5] S. P. Gross, M. Vershini, and G. T. Shubeita. Cargo transport: Two motors are sometimes better than one. *Current Biology*, 17(12):R478–R486, 2007.
- [6] W. O. Hancock and J. Howard. Kinesin’s processivity results from mechanical and chemical coordination between the atp hydrolysis cycles of the two motor domains. *Proceedings of the National Academy of Sciences*, 96(23), 1999.
- [7] C. B. Korn, S. Klumpp, R. Lipowsky, and U. S. Schwarz. Stochastic simulations of cargo transport by processive molecular motors. *The Journal of chemical physics*, 131(24):12B624, 2009.
- [8] J. Newby. Molecular motor-based models of random intermittent search in dendrites. 2010.
- [9] J. Newby, J. L. Schiller, T. Wessler, J. Edelstein, M. G. Forest, and S. K. Lai. A blueprint for robust crosslinking of mobile species in biogels with weakly adhesive molecular anchors. *Nature communications*, 8(1):833, 2017.
- [10] Y. Y. Wang, A. Kannan, K. L. Nunn, M. A. Murphy, D. B. Subramani, T. Moench, R. Cone, and S. K. Lai. Igg in cervicovaginal mucus traps hsv and prevents vaginal herpes infections. *Mucosal Immunology*, 34(4):292–294, 2014.
- [11] T. Wessler, A. Chen, S. McKinley, R. Cone, G. Forest, and K. Lai. Using computational modeling to optimize the design of antibodies that trap viruses in mucus. *ACS Infectious Diseases*, 2(1):82–2, 2016.
- [12] P. Zhu, J. Liu, J. Bess, E. Chertova, J. Lifson, H. Grise, G. Ofek, K. Taylor, and K. Roux. Distribution and three-dimensional structure of aids virus envelope spikes. *Nature*, 441(7095):847–52, 2006.